FTIR Study of Conformational Substates in the CO Adduct of Cytochrome *c* Oxidase from *Rhodobacter sphaeroides*†

David M. Mitchell,‡ Joachim D. Müller,‡ Robert B. Gennis,‡ and G. Ulrich Nienhaus*,‡,§

Departments of Biochemistry and Physics, University of Illinois at Urbana−Champaign, Urbana, Illinois 61801, and Department of Biophysics, Universität Ulm, D-89069 Ulm, Germany

Received July 15, 1996; Revised Manuscript Received October 22, 1996⊗

ABSTRACT: Fourier transform infrared (FTIR) spectroscopy of cytochrome *c* oxidase from *Rhodobacter sphaeroides* reveals multiple CO stretch bands that are associated with different conformational substates of the enzyme. Here we report the temperature dependence of the infrared bands for the CO bound to the Fe_{a_3} heme iron and to Cu_B. We have also studied the kinetics of ligand return from Fe_{a_3} to Cu_B using temperature derivative spectroscopy (TDS). Two classes of substates (α/β) can be distinguished from their different properties with regard to the width of the IR band, the temperature dependence of the peak position, and the peak of the enthalpy distribution. The pronounced temperature dependence of the stretch frequencies in the β conformation and the lack thereof in the α conformation implies very different dynamic behavior in the active site and reflects structural differences between the two conformations, most likely a shift of the position of Cu_B in response to a change in its stereochemical environment. Similar conformational changes will be necessary during the catalytic cycle of the enzyme when dioxygen is bound in the active site.

1. INTRODUCTION

Cytochrome *c* oxidase is a redox-gated proton pump (Babcock & Wikström, 1992; Wikström et al., 1994; Iwata et al., 1995; Rich, 1995). This integral membrane protein catalyzes the one-electron oxidation of ferrocytochrome *c* and the four-electron reduction of dioxygen to water. The free energy made available from the redox reaction is utilized to pump protons electrogenically across the membrane (1 H^+/e^- or 4 H^+/O_2). Cytochrome *c* oxidase is the terminal component of the aerobic respiratory chain in the inner mitochondrial membrane of eukaryotes, and phylogenetically related enzymes are the terminal oxidases in most prokaryotic respiratory chains (Calhoun et al., 1994; Garcia-Horsman et al., 1994). All of these enzymes are members of a large superfamily of heme-copper oxidases (Garcia-Horsman et al., 1994; Saraste & Castresana, 1994; van der Oost et al., 1994; Castresana & Saraste, 1995) named for their unique bimetallic center where oxygen binds and is reduced to water. They have in common a highly conserved transmembrane subunit that provides the amino acid ligands to the high-spin heme iron (Fe_{a_3}) and copper (Cu_B) that comprise the heme-copper center, as well as the ligands for a second, low-spin heme component of these enzymes.

The high-resolution X-ray structures of the cytochrome *c* oxidases from *Paracoccus denitrificans* (Iwata et al., 1995) and from bovine (Tsukihara et al., 1995, 1996) have recently been reported. These two enzymes contain the same redox-active prosthetic groups: (i) a binuclear copper center (Cu_A) located with subunit II; (ii) a low-spin heme *a*, located within subunit I; (iii) the heme a_3/Cu_B bimetallic center, also located within subunit I. Whereas the bovine oxidase contains 13 subunits, the bacterial enzyme contains only four subunits. However, three of the subunits of the bacterial oxidase are homologous to the mitochondrially encoded subunits I, II, and III of the eukaryotic enzyme. The core of the membrane-buried part of these enzymes is provided by the transmembrane helices of subunit I, containing the amino acid residues ligated to heme *a* and the heme a_3/Cu_B center. The X-ray structures of these two enzymes (Iwata et al., 1995; Tsukihara et al., 1995) are very similar with respect to the active site and confirm that the residues in the immediate vicinity of the heme-copper center are highly conserved.

Low-temperature Fourier transform infrared (FTIR) absorption difference spectroscopy of CO bound to the fully reduced enzyme has revealed several important properties of the heme-copper center (Alben et al., 1981; Fiamingo et al., 1986; Shapleigh et al., 1992; Hosler et al., 1994). The initial adduct contains one molecule of CO bound to the heme a_3 iron. Photolysis results in the transfer of the CO from Fe_{a_3} to Cu_B, which is located only about 5 Å away (Iwata et al., 1995; Tsukihara et al., 1995). At sufficiently low temperatures, the Cu_B−CO adduct is stable, and the transfer of the CO from Fe_{a_3} to Cu_B can be monitored by subtracting the IR spectra of the sample prior to and following photolysis. The predominant difference that is observed is due to the alteration of the CO stretching mode, which is sensitive to the change in metal ligation and to electrostatic influences. As the temperature of the sample is increased, the CO dissociates thermally from Cu_B and returns back to Fe_{a_3}. The detailed kinetics of this process can also be monitored by FTIR difference spectroscopy.

Of particular interest is the fact that the IR absorption of CO bound to Fe_{a_3} and to Cu_B is split into multiple bands which represent distinct conformational substates of the oxidase. The two main bands are denoted the α and β

† This work was supported by grants from the National Institutes of Health (GM 18051 and HL16101).

* Send correspondence to this author at Universität Ulm.
‡ University of Illinois.
§ Universität Ulm.

⊗ Abstract published in *Advance ACS Abstracts,* December 1, 1996.

S0006-2960(96)01722-9 CCC: $12.00

substates. They were first seen in the bovine oxidase (Alben et al., 1981; Fiamingo et al., 1986) and later also in the *R. sphaeroides* oxidase (Shapleigh et al., 1992; Cao et al., 1992; Shapleigh & Gennis, 1992; Hosler et al., 1992, 1994). The *R. sphaeroides* oxidase is very closely related to the oxidase from *P. denitrificans*, and the two should have very similar three-dimensional structures.

Similar "taxonomic" substates as the α and β substates in cyt *c* oxidase also occur in the CO adducts of many other heme proteins, like myoglobin (Frauenfelder et al., 1991; Mourant et al., 1993), hemoglobin (Potter et al., 1990), cytochrome P450 (Tsubaki et al., 1986; Porter & Coon, 1991), and horseradish peroxidase (HRP) (Doster et al., 1987; Uno et al., 1987), and in other classes of proteins, for example retinal proteins (Kovacs et al., 1993) or blue copper proteins (Ehrenstein & Nienhaus, 1992; Ehrenstein et al., 1995). Theories suggest that they may be a general property of proteins (Honeycutt & Thirumalai, 1990).

Recent FTIR studies at cryogenic temperatures have demonstrated that the relative populations of α and β substates of the *R. sphaeroides* oxidase depend on environmental conditions, like solvent composition and pH. Under otherwise identical conditions, the β form is favored at low pH (e.g., pH 6), whereas the α form predominates at more alkaline pH values (e.g., pH 8) (Mitchell et al., 1996). Hence, the two substates appear to result from the titration of some group or groups near the metal centers. The protonation and the concomitant conformational changes are sensed by the CO bound to Fe_{a_3} or to Cu_B. Since the mechanism of proton pumping almost certainly involves the protonation/deprotonation of amino acid residues coupled to the redox state of the metals in the heme−copper center, the characterization of the α and β substates is of special interest. Moreover, the relevance of the α and β substates to the catalytic mechanism of the enzyme is also supported by resonance Raman spectroscopy at ambient temperatures (Wang et al., 1995).

In the current work, the dynamics of the heme−copper bimetallic center of the oxidase from *R. sphaeroides* was investigated by FTIR spectroscopy with an experimental protocol called temperature derivative spectroscopy (TDS) (Berendzen & Braunstein, 1990; Mourant et al., 1993). TDS provides information about the enthalpy barriers governing the rebinding of CO to Fe_{a_3} as well as the temperature-dependent changes in the CO environment resulting in shifts of the center frequencies of CO bound to either Cu_B or heme a_3 Fe. Our results indicate that the α and β substates are differentiated by a shift in the position of Cu_B induced by a pH-dependent change in its environment (Wang et al., 1995; Mitchell et al., 1996). Structural changes at the Cu_B site have been suggested as being part of the proton pumping mechanism of the oxidase (Wikström et al., 1994; Iwata et al., 1995).

2. EXPERIMENTAL PROCEDURES

2.1. Sample Preparation

Cytochrome *c* oxidase, modified by a six-histidine affinity tag, was purified from *R. sphaeroides* using Ni-chelate chromatography (Mitchell & Gennis, 1995). The pH was maintained above 8 during all steps of the purification.

Approximately 2.5 mg of purified oxidase was diluted in BIS-TRIS buffer (200 mM, pH 6.5), 0.1% lauryl maltoside, to a total volume of 10 mL. The solution was deoxygenated by repeated cycles of evacuation and CO exposure. Subsequently, sodium dithionite solution was added anaerobically to a final concentration of 20 mM. The protein solution was then centrifuged at 500000*g* for ∼16 h at 4 °C. The supernatant was removed under a CO atmosphere, and the sample was overlaid with CO-saturated glycerol in order to extract excess water from the protein pellet. After a 3−8 h extraction at 4 °C, a small amount of the protein pellet was removed and pressed between two CaF_2 windows separated by an annular spacer of 125 μm.

While most of the data presented in this paper were taken with this "pellet sample" preparation, we have also investigated samples prepared with an alternative procedure, where the purified enzyme (in 50 mM K_2HPO_4 and 0.1% dodecyl maltoside) was concentrated in an Amicon Centricon-30 to ∼500 μM and reduced anaerobically with $Na_2S_2O_4$ solution in the presence of CO gas at 1 atm. Sodium cholate at a final concentration of 1% was also added to the sample to provide a more stable, lipid-like environment for the enzyme upon partial dehydration, which was achieved by flowing dry CO gas for about 10 min over the sample deposited on a sapphire window (diameter 13 mm). Afterward, an annular mylar spacer, thickness 125 μm, and a second window were placed firmly on top. While these "dried samples" also gave excellent infrared spectra, the pellet method was preferred because it consistently yielded higher optical densities.

2.2. Low-Temperature Infrared Spectroscopy

For the measurements, the two sapphire windows holding the sample were enclosed in a block of oxygen-free high-conductivity copper that was mounted on the cold-finger of a closed-cycle helium refrigerator (model 22C, CTI Cryogenics, Waltham, MA). The temperature was regulated with a digital controller (model DRC93C, Lake Shore Cryotronics, Westerville, OH).

Transmittace spectra were collected on a Fourier transform infrared (FTIR) spectrometer (model Sirius 100, Mattson, Madison, WI) between 1800 and 2200 cm^{-1} with a resolution of 2 cm^{-1}. For each spectrum, 280 mirror scans were taken in 200 s. Photodissociation of the samples was achieved by illumination of the samples with light from an argon ion laser with ∼300 mW multimode output (Omnichrome, model 543, Chino, CA). The beam was split and focused with lenses on the samples from both sides.

2.3. Data Collection and Analysis

To measure the temperature dependence of the IR spectra of cyt *c* oxidase with CO ligated to the heme a_3 iron, the sample was cooled in the dark to 12 K. Subsequently, the sample was heated from $T_{min} = 12$ K to $T_{max} = 200$ K linearly in time at a rate $\alpha = 5$ mK/s, so that the ramp temperature, T_R, is given by

$$T_R(t) = T_{min} + \alpha t \qquad (1)$$

During heating, transmittance spectra were taken continuously at a rate of 1 spectrum/K. Subsequently, the sample was cooled again to 12 K, photodissociated completely, and a spectrum was taken as a reference for conversion of all 189 other spectra to absorbance difference spectra.

To examine the temperature dependence of the IR spectra of the CO bound to the Cu_B, the sample was illuminated at 12 K so as to completely photodissociate the CO from the Fe_{a_3} iron to form the Cu_B-CO adduct. Subsequently, the sample was heated in the same fashion as described in the previous paragraph while spectra were taken continuously. By referencing against a 12 K spectrum of the sample cooled in the dark, absorbance difference spectra of the IR bands of the CO bound to Cu_B were calculated.

To analyze the kinetics of the CO returning to the heme a_3 iron, we used temperature derivative spectroscopy (TDS), a kinetic protocol that provides a convenient way of studying thermally activated rate processes (Berendzen & Braunstein, 1990). In this method, absorbance difference spectra, $\Delta A(\nu,T_R)$, are calculated from successive transmittance spectra, $I(\nu,T_R)$, collected during a temperature ramp after complete photodissociation of the sample at 12 K.

$$\frac{dA}{dT_R} \approx \Delta A(\nu,T_R) = \log I(\nu,T_R - {}^1/_2\text{K}) - \log I(\nu,T_R + {}^1/_2\text{K}) \quad (2)$$

Hence, the same transmittance spectra are being used as in the preceding paragraph. There, however, all spectra were referenced to a 12 K dark spectrum. A successive difference spectrum, $\Delta A(\nu,T_R)$, represents the amount of rebinding at the temperature T_R in the time interval between the two transmittance spectra, assuming that the absorbance can be taken as proportional to the number of molecules that have rebound. Note that this statement is only correct if temperature-dependent changes between consecutive spectra can be neglected in comparison with the rebinding signal. Calculation of successive differences is actually an approximate procedure that yields (after normalization) the negative derivative of the photolyzed fraction with respect to the ramp temperature, $-dN/dT_R$. Assuming a functional form, for example a Gaussian, the distribution of rebinding barriers, $g(H)$, can be calculated from the TDS signal, $-dN/dT_R$, as described previously (Berendzen & Braunstein, 1990; Mourant et al., 1993).

TDS measures rebinding at a constant rate, which is the inverse of a characteristic time, τ_c, as a function of ramp temperature T_R. CO rebinding to Fe_{a_3} at low temperatures is a first-order process and occurs by thermal activation over an enthalpy barrier, H. Therefore, the rate, barrier height and temperature are connected by the Arrhenius law. Thus, the activation enthalpy, H, of the population rebinding at T_R can be calculated by (Berendzen & Braunstein, 1990)

$$H = RT_R \ln(A\tau_c) \quad (3)$$

where R denotes the gas constant, A is the Arrhenius preexponential, and the characteristic time τ_c is given by

$$\tau_c = \frac{RT_R^3}{\alpha T_0(H + RT_R)} \quad (4)$$

Here, T_0 is a reference temperature of 100 K. The preexponential, A, has to be determined independently by time-resolved experiments.

For the quantitative analysis of the absorbance difference spectra, their baselines were fitted with a polynomial which was then subtracted. The areas and band positions of the CO stretch bands were determined by fitting convolutions of Gaussians and Lorentzians (Voigtians) to the spectra.

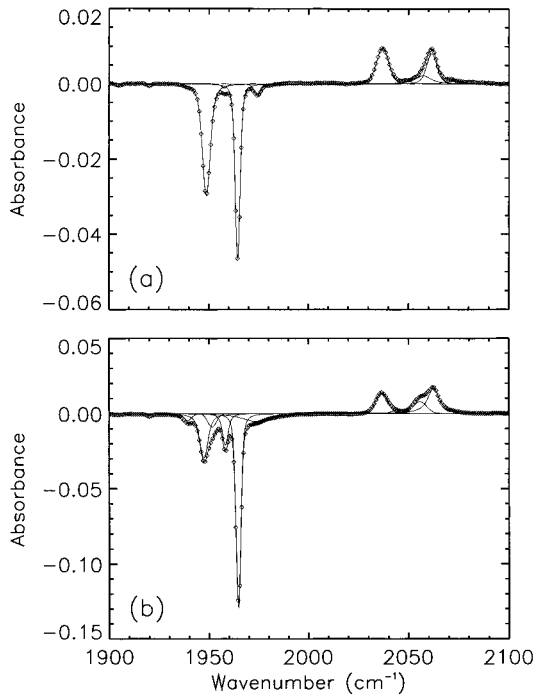

FIGURE 1: Dark-minus-light Fourier transform difference spectra of *R. sphaeroides* cyt *c* oxidase at 12 K, (a) dried sample, and (b) pellet sample. Diamonds, experimental data; solid lines, fit with Voigtians (see Table 1 for the parameters).

Table 1: Parameters of Sum-of-Voigtian Fits to the CO Stretch Spectra in Figure 1

sample	substate	area (OD cm^{-1})	position (cm^{-1})	width (cm^{-1})
dried	β_{1947}	−0.183	1948.6	4.8
	α_{1958}	−0.006	1957.7	3.2
	α_{1964}	−0.171	1964.4	3.0
	α_{1974} [a]	−0.014	1974.3	3.9
	β_{2037}	0.080	2037.1	7.3
	α [b]	0.033	2057.3	9.4
	α_{2062}	0.061	2061.5	6.0
	α [b]	0.012	2072.4	10.6
pellet	β_{1939}	−0.028	1939.3	4.6
	β_{1947}	−0.203	1947.3	5.0
	β [b]	−0.050	1951.5	5.2
	α_{1958}	−0.100	1958.2	3.5
	α_{1964}	−0.461	1964.7	3.0
	α_{1974} [a]	−0.130	1973.2	16.4
	β_{2037}	0.102	2036.5	7.1
	β [b]	0.009	2043.5	5.8
	α [b]	0.065	2055.7	7.8
	α_{2062}	0.176	2062.4	7.0

[a] Tentative assignment. [b] Within the envelope of a neighboring band and not assigned to a separate substate.

3. RESULTS

Figure 1 shows the dark-minus-light absorbance spectra of cyt *c* oxidase at 12 K for two samples prepared with the different techniques described in subsection 2.1. Experimental data are given as points, whereas the model calculations with sums of Voigtians are represented as solid lines. The fit parameters are compiled in Table 1. The spectrum of the dried sample in Figure 1a is dominated by two negative IR bands at 1948 and 1964 cm^{-1} that arise from the stretch vibration of the CO bound to Fe_{a_3}. Compared with other IR

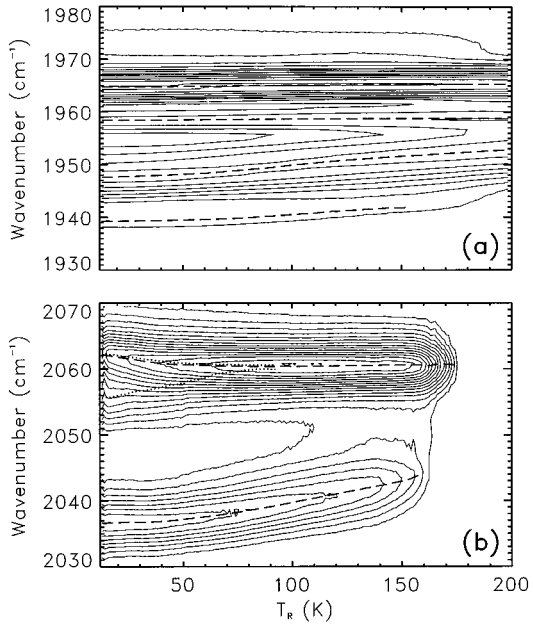

FIGURE 2: Contour plot of the CO stretch absorption as a function of wavenumber and temperature. (a) CO bound to Fe_{a_3}, (b) CO bound to Cu_B. Dashed lines, peak wavenumber of the different bands; dotted lines, peak wavenumbers when fitting α_{2062} with two bands. For details, see the text. Contours are spaced logarithmically.

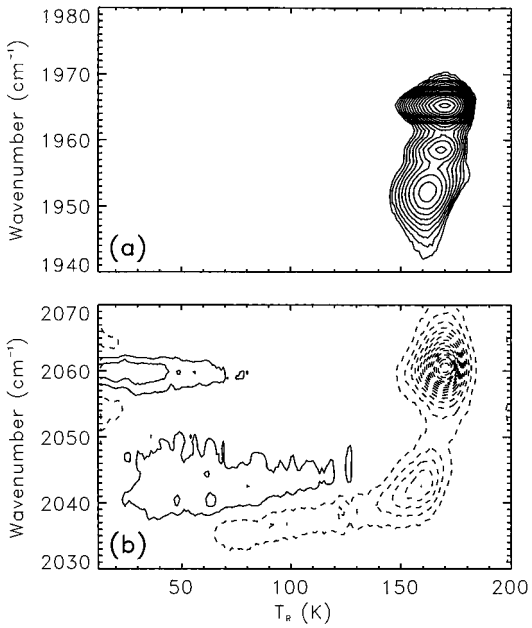

FIGURE 3: TDS contour map calculated from the data in Figure 2, with positive contours as solid lines, and negative contours as dashed lines; (a) CO bound to Fe_{a_3}, (b) CO bound to Cu_B. Contours are spaced logarithmically.

bands of CO in proteins, the band at 1964 cm^{-1} is remarkably sharp (FWHM 2.5 cm^{-1} as measured at a spectrometer resolution of 0.5 cm^{-1}). Close inspection reveals two minor bands at 1958 and 1974 cm^{-1}. The two small peaks at 1904 and 1920 cm^{-1} are due to the small natural abundance of the $^{13}C^{16}O$ isotope. The two positive IR bands at 2037 and 2062 cm^{-1} arise from CO that is bound to Cu_B after photodissociation from Fe_{a_3}. To get a good fit of the band at 2062 cm^{-1}, additional lines at 2057 and 2072 cm^{-1} were necessary. In mammalian cyt *c* oxidase, these multiple CO stretch bands have been explained with the existence of different conformational substates, called α and β substates (Fiamingo et al., 1986). The α substate is characterized by the very narrow IR stretch band at 1964 cm^{-1} in the Fe-bound form and at 2062 cm^{-1} in the Cu_B-bound form, while the β substates absorbs at 1948 cm^{-1} in the Fe-bound form, and at 2037 cm^{-1} in the Cu_B-bound form.

The spectrum of the pellet sample in Figure 1b also shows the α and β substate lines. However, the presence of minor bands is even more obvious than in the dried sample. For the Fe-bound CO, the minor bands are located at 1939, 1958, and 1973 cm^{-1}. The β band at 1947 cm^{-1} has a pronounced asymmetry toward higher wavenumbers, and to achieve a good fit, an additional line at 1951 cm^{-1} is needed. In the stretch bands of the Cu-bound CO, the fit of the β band at 2037 cm^{-1} can be improved by adding an additional, weak band at 2043 cm^{-1}. Furthermore, on the left wing of the α band at 2062 cm^{-1}, a separate band at 2056 cm^{-1} appears. This band is much more obvious here than in the dried sample (compare with Figure 1a).

While the 12 K spectra yield rich information about the existence of various bands, more insights can be gained from the temperature dependence of the IR spectra. Figure 2 shows two-dimensional contour maps of the absorbance spectra obtained with the pellet sample, plotted as a function of temperature. In Figure 2a, the region of the Fe-bound CO stretch bands is plotted. Also included are the peak positions of the most prominent bands as dashed lines. For these fits, the peaks at 1947 and 1951 cm^{-1} have been combined in a single β band. The α band at 1964 cm^{-1} shows a very weak temperature dependence. From 12 to 200 K it shifts by only 0.4 cm^{-1} toward higher wavenumbers. The peak at 1958 cm^{-1} has the same weak temperature dependence. By contrast, the β band at 1947 cm^{-1} shows a much larger upshift, from 1947 cm^{-1} at 12 K to 1953 cm^{-1} at 200 K. This shift continues to 1955 cm^{-1} at room temperature (Wang et al., 1995). A very similar temperature dependence is obtained for the band at 1939 cm^{-1} up to 150 K. Above this temperature, this band becomes so broad and shifts toward higher wavenumbers so that it can no longer be resolved unambiguously. The band at 1973 cm^{-1} is very broad in the pellet sample; the contours in Figure 2a indicate, however, that its position stays fairly constant up to at least 180 K.

The contours of the Cu-bound CO stretch spectra are shown in Figure 2b. They disappear above 150 K because the CO dissociates thermally from Cu_B and rebinds to Fe_{a_3}. Again, the dashed lines indicate a pronounced difference in the temperature dependence of the α and β bands. For the α band at 2062 cm^{-1}, the peak position shown by the dashed line was determined by fitting a single Voigtian. When fitting the two lines at 2055 and 2062 cm^{-1} separately (dotted lines), the line at 2062 cm^{-1} shifts down by 2 wavenumbers up to 70 K, while the line at 2055 cm^{-1} shifts up and merges. Above 70 K, the position of the line stays temperature independent. By contrast, the band at 2037 cm^{-1} is much more affected by temperature and shifts to 2043 cm^{-1} at 150 K.

Figure 3 shows the TDS signal, i.e., the integrated absorbance differences between spectra taken at successive temperatures. The contours in Figure 3a represent spectral changes of the Fe-bound CO due to recombination in the temperature range 150−170 K. Figure 3b shows the corresponding data as measured in the Cu-bound CO stretch

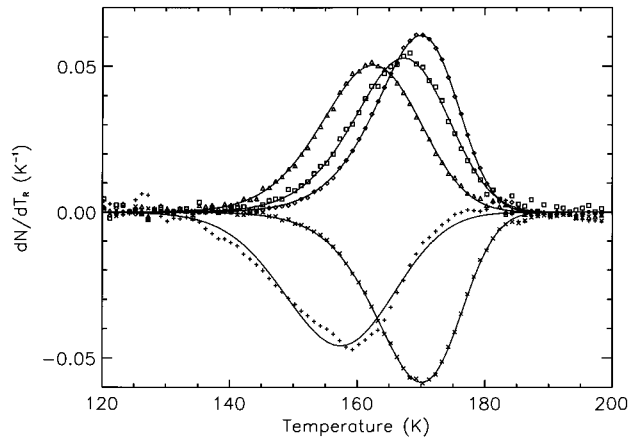

FIGURE 4: TDS signal as a function of ramp temperature T_R for the various peaks, obtained by integrating the absorbance in the specified wavenumber intervals. Diamons, α_{1964} (slice from 1964 to 1966 cm^{-1}); triangles, β_{1947} (slice from 1950 to 1955 cm^{-1}); squares, α_{1958} (slice from 1957.5 to 1959.5 cm^{-1}); crosses, α_{2061} (slice from 2060 to 2065 cm^{-1}); pluses, β_{2037} (slice from 2030 to 2048 cm^{-1}). The solid lines are fits of a Gaussian enthalpy barrier distribution to the data.

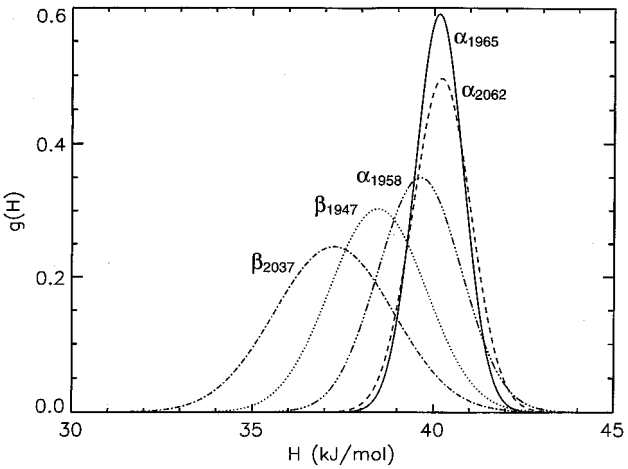

FIGURE 5: Enthalpy distributions obtained from the fit to the data in Figure 4.

Table 2: Fit Parameters of the Gaussian Activation Enthalpy Distributions Shown in Figure 5

substate (cm^{-1})	H_{peak} (kJ/mol)	width (FWHM) (kJ/mol)
β_{1951}	38.5	3.1
α_{1958}	39.6	2.7
α_{1964}	40.1	1.6
β_{2037}	37.3	3.8
α_{2062}	40.2	1.9

bands. Again, the dominant features are due to recombination of the CO between 150 and 170 K. They have the opposite sign of the Fe-bound bands, indicated by the dashed lines, because absorbance loss in the Cu−CO bands upon ligand return is accompanied by absorbance gain in the Fe-bound states. Additional features in the Cu−CO maps represent the large, temperature-dependent spectral changes. The signal around 2060 cm^{-1} below 50 K arises from the shift of the 2055 and 2062 cm^{-1} bands, whereas the extended features in the β bands below 2050 cm^{-1} arise from the continuous, strong upshift.

For a quantitative analysis of the TDS data, we have integrated the absorbance differences within wavenumber intervals that cover the different bands. These data are plotted in Figure 4 together with fits that are shown as solid lines. The wavenumber intervals are given in the caption of the figure. For the fits, we have assumed a unimodal, Gaussian distribution of enthalpy barriers, $g(H)$, and a pre-exponential $A = 10^9$ s^{-1}, as obtained from measurements on bovine cyt *c* oxidase (Fiamingo et al., 1982). The fits match up very well with the data points, implying that the assumption of a Gaussian distribution is appropriate. This kind of distribution is often found in ligand binding experiments at cryogenic temperatures (Ehrenstein & Nienhaus, 1992). The enthalpy distributions resulting from the fit are plotted in Figure 5, and the fit parameters are listed in Table 2.

4. DISCUSSION

The present study on cyt *c* oxidase gives further evidence that conformational substates in proteins are arranged in a hierarchical fashion (Frauenfelder et al., 1991). A few taxonomic substates can be identified by their different CO stretch bands. Within each of these, a multitude of substates exists, as evidenced by the distribution of rebinding barriers, $g(H)$ (Figure 5).

The dominant α and β substates have distinctly different properties, and the pH dependence of the relative populations of α and β substates implies that they are connected to the titration of a residue close to the active site (Mitchell et al., 1996). The CO stretch of the α substate at 1964 cm^{-1} is extremely narrow compared with the CO stretch in other heme proteins (Alben et al., 1982; Potter et al., 1990; Mourant et al., 1993), suggesting a rigid environment that constrains the ligand. This property is also reflected in the weak temperature dependence of both the Fe and Cu_B-bound CO in the α substate, as shown in Figure 2. The behavior of the α substate peak in the Cu-ligated form is very interesting. Figure 2b shows that it is constant at 2061 cm^{-1} between 80 and 170 K, but splits into two bands below 80 K. The population-weighted average of the two peaks stays at 2061 cm^{-1}, which implies that the collapse of the two peaks into one with increasing temperature occurs because of rapid (picosecond time scale) exchange between two conformational states. To explain the high interconversion rate between the two peaks in mammalian cyt *c* oxidase, Alben and collaborators have suggested an exchange process where a proton can assume two positions between an ionizable ligand of Cu_B and an adjacent ionizable residue of the protein (Fiamingo et al., 1990). The absence of this splitting in the β form would then imply a different arrangement of the hydrogen bonds in that conformation. The β substate has a pronounced shift of the CO stretch bands between 12 and 150 K: $\Delta\nu = 5$ cm^{-1} for the Fe-bound CO and 7 cm^{-1} for the Cu_B-bound CO. These large, temperature-dependent shifts indicate that interactions between the CO and neighboring atoms in the active site are strongly modulated by thermal motions and that the active site in the β substate is indeed very flexible.

Particularly interesting in the present study is the characterization of the minor bands. From their spectral shapes, spectral temperature dependencies, and kinetic properties, we can classify them as either α and β substates. To distinguish the different states, we use the band positions at 12 K as labels to denote the states. These labels are also

included in Table 1. Hence, the "normal" Fe-bound α substate band will be called α_{1964}.

The band at 1958 cm^{-1} is also very narrow and has the weak temperature dependence of α_{1964}, as shown in Figure 2. The barrier distribution, $g(H)$, is also close to that of α_{1964}. Therefore, we call this band α_{1958}. By contrast, the peak at 1939 cm^{-1} is comparable in width to β_{1948} and also mimicks its temperature dependence. In the TDS contour map, Figure 3a, it is not as well separable from the other peaks as α_{1958}. However, the shape of the tail of the contours towards lower wavenumbers indicates that the recombination of this peak is similar to that of β_{1948}. Therefore, we denote this minority species as β_{1939}. The species at 1974 cm^{-1} in the dried sample has a narrow width of 3.9 cm^{-1}. In the pellet sample, the peak is exceedingly broad (16.4 cm^{-1}), however. The contour map in Figure 2a shows a weak temperature dependence, which would classify it as an α substate. Considering the width of the band, we can only make a tentative assignment in this case.

How can we explain these peaks in structural terms? The titration of a crucial residue at the active site gives rise to a splitting into an α and β species with very distinct properties. The pK of this transition can be shifted by mutations in the vicinity of the active site (Mitchell et al., 1996). Clearly, there must be other structural influences that lead to a further splitting into α_{1958} and α_{1964}, β_{1939} and β_{1948}, and possibly even more states. Since the water activity of the dried and pellet samples is very different, one could speculate about the presence and absence of water molecules in the vicinity of the active site or about titrations of other residues. Note that the species represented by the different IR bands of the Fe_{a_3}-bound CO are not in dynamic equilibrium, but are frozen into their respective states in the temperature range studied. This is evident from the fact that the recombination process occurs at different temperatures, or equivalently, with different barrier distributions.

The dominant α and β substates of the CO adduct of cytochrome aa_3 have recently been investigated with Raman spectroscopy on both the C−O and Fe−C stretch at room temperature (Wang et al., 1995). On the basis of Raman and IR data on many heme proteins and model heme, a linear correlation between the C−O and Fe−CO stretch frequencies has been established empirically (Li & Spiro, 1988; Ray et al., 1994). The underlying physical mechanism for this behavior was identified as Fe → CO backbonding that simultaneously strengthens the Fe−C bond and weakens the C−O bond. While the β substate lies on the correlation curve, the α substate deviates markedly (Hosler et al., 1994). This anomalous behavior is also seen in mammalian cyt *c* oxidase and cytochrome bo_3 (Wang et al., 1995, and references therein). A number of explanations have been put forward over the past few years involving the proximal side of the heme (Argade et al., 1984; Rousseau et al., 1993). More recently, with the work Cu_B-deficient mutants implied that the distal environment may be responsible for the position of the oxidases off the frequency correlation (Hosler et al, 1994; Uno et al., 1994).

How does the distal environment affect the Fe−CO and C−O stretch frequencies? IR spectroscopy with a variety of distal pocket mutants of myoglobin revealed that mainly electrostatic interactions are responsible for these changes (Braunstein et al., 1993; Li et al., 1994). The backbonding mechanism responsible for the correlation between ν_{Fe-CO} and ν_{C-O} ensures that the changes in ν_{C-O} are accompanied by the appropriate changes in ν_{Fe-CO}. As an example, the A substates at 1930, 1945, and 1966 cm^{-1} in sperm whale MbCO (Mourant et al., 1993) obey the correlation quite nicely (Ray et al., 1994). Therefore, the deviation of the α substate cannot be explained purely on the basis of electrostatic interactions with the distal pocket. Since it occurs in all heme/copper terminal oxidases, the most likely explanation involves Cu_B at a distance of ∼5 Å from heme a_3 Fe (Iwata et al., 1995), close enough to interact with the Fe−CO unit. This interaction would also confine the CO to a much more restricted position than the one usually found in heme proteins.

In the β substate, by contrast, ν_{Fe-CO} and ν_{C-O} lie on the backbonding correlation. If we are correct that Cu_B interacts strongly with the Fe-bound CO in the α conformation, the normal behavior in the β form would imply that Cu_B is further removed from the Fe-bound CO ligand. The pH dependence of the relative α and β substate populations indicates that this structural change is connected to the titration of a nearby residue. In the recently published structure of a homologous oxidase of *P. denitrificans*, His 325 (His 333 in our protein) was assumed to become protonated in the catalytic cycle and to serve as a proton shuttle (Iwata et al., 1995). If the α/β interconversion would correspond to one of the histidine ligands of Cu_B protonating and dissociating from the metal, we would expect that the low pH β form should have the higher frequency because removal of a basic ligand should increase the frequency as the extent of backbonding decreases. Consequently, we conclude that the protonation and concomitant structural changes do not happen in the first coordination shell of Cu_B, but rather in the network of hydrogen bonds stabilizing the histidine ligands.

Finally, we briefly discuss the rebinding of the CO to Fe_{a_3}. This reaction is characterized by enthalpy barriers distributed around 40 kJ/mol (see Figure 5 and Table 2) with full widths at half-maximum between 1.9 and 3.8 kJ/mol. The presence of barrier distributions indicates that each of the α and β substates consists of a distribution of substates in the lower tiers of the hierarchy (Frauenfelder et al., 1991). Compared with other heme proteins, the barriers are very high in cyt *c* oxidase, whereas the distributions are narrow. For example, the dominant A_1 substate in sperm whall MbCO has a peak enthalpy of 10 and a width of 7 kJ/mol (Steinbach et al., 1991; Johnson et al., 1996). This difference may arise from the fact that, in cyt *c* oxidase, the CO binds to Cu_B, and the recombination kinetics are governed by the dissociation of the CO from Cu_B, and thus association with Fe_{a_3} is not rate limiting. Consequently, the TDS signals observed in the Fe_{a_3}-bound CO lines should yield the same barrier distributions as those in the Cu_B-bound CO lines. Within the error of the data, this is the case for the α substates. Figure 4 shows, however, that the Cu_B-bound CO line (β_{2037}) starts to decay already before the corresponding Fe_{a_3}-bound CO line (β_{1947}) begins to increase. This observation implies that at least some of the CO molecules dissociating from Cu_B do not immediately recombine with Fe_{a_3}, but stay free in the pocket and recombine with Fe_{a_3} at a higher temperature. For these molecules, the association would govern the return rate. Clearly, further work is necessary to elucidate the kinetic details of this reaction.

We have studied the temperature dependence of the IR stretch bands of CO bound to both the Fe_{a_3} heme iron and Cu_B in cyt *c* oxidase. The observed bands represent different conformational substates that fall into two classes (α/β). The pronounced temperature dependence of the stretch frequencies in the β conformation and the lack thereof in the α conformation implies very different dynamic behavior in the active site and suggests also a conformational change between the two conformations, most likely a shift of the position of Cu_B (Wang et al., 1995; Mitchell et al., 1996). So far, these taxonomic α and β substates have only been detected in the CO adduct of oxidase. However, similar conformational changes will be necessary during the catalytic cycle of the enzyme, and further investigations of CO-bound oxidase may yield important information for the proton pumping mechanism of the enzyme.

ACKNOWLEDGMENT

We thank Dr. Alben of The Ohio State University for helpful discussions.

REFERENCES

Alben, J. O., Moh, P. P., Fiamingo, F. G., & Altschuld, R. A. (1981) *Proc. Natl. Acad. Sci. U.S.A. 78*, 234−237.

Alben, J. O., Beece, D., Bowne, S. F., Doster, W., Eisenstein, L., Frauenfelder, H., Good, D., McDonald, J. D., Marden, M. C., Moh, P. P., Reinisch, L., Reynolds, A. H., Shyamsunder, E., & Yue, K. T. (1982) *Proc. Natl. Acad. Sci. U.S.A. 78*, 2903−2907.

Babcock, G. T., & Wikström, M. (1992) *Nature 356*, 301−309.

Berendzen, J., & Braunstein, D. (1990) *Proc. Natl. Acad. Sci. U.S.A. 87*, 1−5.

Calhoun, M. W., Thomas, J. W., & Gennis, R. B. (1994) *Trends Biochem. Sci. 19*, 325−330.

Cao, J., Hosler, J., Shapleigh, J., Revzin, A., & Ferguson-Miller, S. (1992) *J. Biol. Chem. 267*, 24273−24278.

Castresana, J., & Saraste, M. (1995) *Trends Biochem. Sci. 20*, 443−448.

Doster, W., Bowne, S. F., Frauenfelder, H., Reinisch, L., & Shyamsunder, E. (1987) *J. Mol. Biol. 194*, 299−312.

Ehrenstein, D., & Nienhaus, G. U. (1992) *Proc. Natl. Acad. Sci. U.S.A. 89*, 9681−9685.

Ehrenstein, D., Filiaci, M., Scharf, B., Engelhard, M., Steinbach, P. J., & Nienhaus, G. U. (1995) *Biochemistry 34*, 12170−12177.

Fiamingo, F. G., Altschuld, R. A., Moh, J. O., & Alben, J. O. (1982) *J. Mol. Chem. 257*, 1639−1650.

Fiamingo, F. G., Altschuld, R. A., & Alben, J. O. (1986) *J. Biol. Chem. 261*, 12976−12987.

Fiamingo, F. G., Jung, D. W., & Alben, J. O. (1990) *Biochemistry 29*, 4627−4633.

Frauenfelder, H., Sligar, S. G., & Wolynes, P. G. (1991) *Science 254*, 1598−1603.

Garcia-Horsman, J. A., Barquera, B., Rumbley, J., Ma, J., & Gennis, R. B. (1994) *J. Bacteriol. 176*, 5587−5600.

Honeycutt, J. D., & Thirumalai, D. (1990) *Proc. Natl. Acad. Sci. U.S.A. 87*, 3526−3529.

Hosler, J. P., Fetter, J., Tecklenberg, M. M. J., Espe, M., Lerma, C., & Ferguson-Miller, S. (1992) *J. Biol. Chem. 267*, 24264−24272.

Hosler, J. P., Kim, Y., Shapleigh, J., Gennis, R., Alben, J., Ferguson-Miller, S., & Babcock, G. (1994) *J. Am. Chem. Soc. 116*, 5515−5516.

Iwata, S., Ostermeier, C., Ludwig, B., & Michel, H. (1995) *Nature 376*, 660−669.

Johnson, J. B., Lamb, D. C., Frauenfelder, H., Müller, J. D., McMahon, B., Nienhaus, G. U., & Young, R. D. (1996) *Biophys. J. 71*, 1563−1573.

Kovacs, I., Nienhaus, G. U., Philipp, R., & Xie, A. (1993) *Biophys. J. 64*, 1187−1193.

Mitchell, D. M., Shapleigh, J. P., Alben, J. O., & Gennis, R. B. (1996) *Biochemistry 35*, 9446−9450.

Mourant, J. R., Braunstein, Chu, K., Frauenfelder, H., Nienhaus, G. U., Ormos, P., & Young, R. D. (1993) *Biophys. J. 65*, 1496−1507.

Porter, T. D., & Coon, M. J. (1991) *J. Biol. Chem. 266*, 13469−13472.

Potter, W. T., Hazzard, J. H., Choc, M. G., Tucker, M. P., & Caughey, W. S. (1990) *Biochemistry 29*, 6283−6295.

Rich, P. R. (1995) *Aust. J. Plant Physiol. 22*, 479−486.

Saraste, M., & Castresana, J. (1994) *FEBS Lett. 341*, 1−4.

Shapleigh, J. P., & Gennis, R. B. (1992) *Mol. Microbiol. 6*, 635−642.

Shapleigh, J. P., Hill, J. J., Alben, J. O., & Gennis, R. B. (1992) *J. Bacteriol. 174*, 2338−2343.

Steinbach, P. J., Ansari, A., Berendzen, J., Braunstein, D., Chu, K., Cowen, B. R., Ehrenstein, D., Frauenfelder, H., Johnson, B., Lamb, D. C., Luck, S., Mourant, J. R., Nienhaus, G. U., Ormos, P., Philipp, R., Xie, A., & Young, R. D. (1991) *Biochemistry 30*, 3988−4001.

Tsubaki, M., Hiwatashi, A., & Ichikawa, Y. (1986) *Biochemistry 35*, 3563−3569.

Tsukihara, T., Aoyama, H., Yamashita, E., Tomizaki, T., Yamaguchi, H., Shinzawa-Itoh, K., Nakashima, T., Yaono, R., & Yoshikawa, S. (1995) *Science 269*, 1069−1074.

Tsukihara, T., Aoyama, H., Yamashita, E., Takashi, T., Yamaguchi, H., Shinzawa-Itoh, K., Nakashima, T., Yaono, R., & Yoshikawa, S. (1996) *Science 272*, 1136−1144.

Uno, T., Nishimura, Y., Tsuboi, M., Makino, R., Iizuka, T., & Ichikawa, Y. (1987) *J. Biol. Chem. 262*, 4549−4556.

van der Oost, J., deBoer, A. P. N., deGier, J.-W. L., Zumft, W. G., Stouthamer, A. H., & van Spanning, R. J. M. (1994) *FEMS Microbiol. Lett. 121*, 1−9.

Wang, J., Takahashi, S., Hosler, J. P., Mitchell, D. M., Ferguson-Miller, S., & Rousseau, D. L. (1995) *Biochemistry 34*, 9819−9825.

Wikström, M., Bogachev, A., Finel, M., Morgan, J. E., Puustinen, A., Raitio, M., Verkhovskaya, M., & Verkhovsky, M. I. (1994) *Biochim. Biophys. Acta 1187*, 106−111.

BI961722Z